SCIENTIFIC PAPER

Simplifying the human lumbar spine (L3/L4) material in order to create an elemental structure for the future modeling

Neda Salsabili[1] · Joaquín Santiago López[1] · María Isabel Prieto Barrio[1]

Abstract

The human lumbar spine incorporates the best joints in nature due to its optimal static and dynamic behavior against the internal and external loads. Developing an elemental structure based on this joint requires simplification in terms of the materials employed by keeping the mechanical and anatomical behaviors of the human lumbar spine. In the present study, the finite element (FE) of two motion segments of the human lumbar spine (L3/L4) was developed based on the CT scan data as the base for vertebrae geometry, verified geometry properties for another part of two motion segments, and combination of materials and loads obtained from the validated resources. Then, simplification occurred in four continuous steps such as omitting the annual fibers of annual matrix, representing the material of the annual matrix to the nucleus, demonstrating the material of annual matrix to the endplates too, and omitting the trabecular part of vertebrae. The present study aimed to propose the method for developing the basic structure of the human lumbar spine by simplifying its materials in the above-mentioned steps, analyzing the biomechanical effects of these four steps in terms of their internal and external responses, and validating the data obtained from the FE method. The validated simplified way introduced in this study can be used for future research by making implants, prosthesis, and modeling based on the human lumbar spine in other fields such as industrial design, building structures, or joints, which results in making the model easier, cheaper, and more effective.

Introduction

Bionic architecture as a main field of Bionics tries to design and construct the buildings based on layout and lines of natural forms [1]. Nature has inspired the architecture by focusing on mimicking the geometrical principles embedded in nature in terms of the aesthetics and economics of geometric interventions [1]. During the twenty-first century, the movement was matured by incorporating the biological, mathematical and mechanical principles of nature to architectural design [2], which is known as the architecture derived from nature [3]. It is worth noting that this field becomes more significant in the era of ecological crisis for the purpose of adaptability and flexibility, which is formed within the course of natural evolution, flexible forms, and structure which could be rectified through the changes of

natural evolution proven to be the most efficient sources of inspiration [1, 2, 4].

The human spine joint is considered as a perfect example of flexible and adapted natural structures similar to other human joints (the frame of the human body). The spine joint has six key features including aesthetics by harmonizing in response to environmental forces [5, 6], complexity by adapting to flexion, extension, abduction, adduction, rotation, and circumduction movements simultaneously [6], comfort created by ensuring stability in different positions, dynamism by facilitating the balance through flexible movements [3, 6], light structural system, and modular form [3, 7]. The roles performed by the spine joint are very similar to the type of role required within the building and industrial design. Thus, it is considered as a natural element which can inform the future of architecture and industrial design. The spine joint as the most important and biggest structure of the human body joints system consists of vertebrae (cortical and trabecular part), intervertebral discs (annuals matrix, annuals fibers, and nucleus part), ligaments (seven types of ligaments), and facet joints [8]. Nowadays, it is possible

✉ Neda Salsabili
 n.salsabili@gmail.com; n.salsabili@alumnos.upm.es

[1] Escuela Técnica Superior de Edificación, Universidad Politécnica de Madrid, Madrid, Spain

to simulate [8] the sustainable systems with increased efficiency by recognizing the spine joints [2, 3, 9]. This simulation is conducted by using the combination of biology, construction, mathematics, mechanics, and computational programs and software [2, 3]. However, the simulation of such structure requires a simplification of both structural and material complexity of the spine joint in accordance with the architectural and construction resources available. This process can ease the process of modeling such structures for the bioengineering and prosthetics industry, as well as other future structures. The present study aimed to indicate the effects of each material of human lumbar spine L3/L4 (which were changed or omitted) on its internal and external response to conduct the simple and basic structure by FE method.

By implementing a different range of properties for modeling different geometrical parts, finite element method (FEM), as a non-invasive and numerical [10, 11] tool in a virtual environment [12–14], can help simulate, analyze [13], and evalaute the effect of simplification of the material parts of human lumbar spine [15–17] easier [18], without any damage to the spine [19], reduce the time, testing [13], physical prototypes [20], and material uses [12], improve the safety and information standards [13], optimize different geometry properties [11, 13, 18, 21] for prosthesis[22] and different physiological conditions [15, 19, 22, 23], measure different distribution of stresses, displacements [18], and load transferring mechanisms [15, 16, 19], and assist in developing the new spinal implants [15]. Thus, this method has more advanatges compared to the vivo methods due to some limitations in terms of measuring, obtaining [24], as well as varying the specimen [19]. In addition, the vivo methods are costly and time-consuming [16, 21].

There are many finite element (FE) simulations for evaluating the biomechanical behavior of the lumbar spine as the largest part of the whole spine which is responsible for the majority of weight bearing and flexible movement functions [25]. Shirazi-Adl developed a FE model of L1–L5 lumbar spine to predict optimal lumbar spine posture and stress in its soft tissues [26]. Little et al. devised a FE model of L1–L5 lumbar spine to study the spinal anatomy and the coupled rotations in the lumbar spine [27]. In addition, Ayturk and Puttlitz created a FE model of L1–L5 lumbar spine [28]. In another study, Schmidt et al. built a FE model of L1–L5 lumbar spine to predict the spine biomechanics after disc implanting [29]. Kiapour et al. developed a FE model of L3–S1 lumbar spine to simulate the muscle forces and upper body weight before loading conditions, predict lumbar spine motion after surgery, and evaluate spine biomechanics after implanting an artificial intervertebral disc [30]. Furthermore, Lin et al. implemented a FE model of L1–L5 lumbar spine to assess the effect of dynamic spinal fixators of the lumbar spine

[31]. Park et al. built a FE model of L1–S1 lumbar spine with both healthy and degenerated intervertebral discs to evaluate the effects of degenerated intervertebral discs on the lumbar spine biomechanics [32].

All of the above models were built based on the CT scan of the one person subject and validated by comparing with experimental data. These models were taken as a prototype in many ways to represent other subjects for applications and predictions [33], capture the internal biomechanical parameters of the bones or connective soft tissues [34], study the effects of pedicle-screw and replacement of artificial discs on lumbar spine biomechanics [33], find the distribution of loads, or check the prosthesis or implanting part which was already designed by FE method.

However, these FE models were not modeled based on material simplification by the FE method. To the best of our knowledge, the present study is the first to analyze the simplification of the materials as a part of the human lumbar spine by FE method, in order to create a simple structure with fewer materials for the aspects of prosthesis and implanting or building joints and structures. In general, FE modeling occurs by simplifying the material parts of two motion segments of human lumbar spine L3/L4 over four continuous steps to analyze the effects of replacing or omitting these material parts on two motion segments. Taken as a basic unit, the two motion segments were used since they can provide a characterization of the whole spine and FE models and contribute to the promotion of quantitative spinal biomechanics studies [15]. Simplifying each part of the two motion segments offers an easier and cheaper way of building a structure with less damage and lower use of materials.

This paper presents a three-step method to examine the feasibility and usefulness of simplifying the material element of the human lumbar while maintaining its mechanical and anatomical properties in FE modeling. First, the FE of lumber was made by using a combination of different software with verified formula, properties, and techniques for calculating the model [33]. Second, the model was validated by comparing its internal and external response with vitro and vivo experimental data [21, 33]. Finally, it was stripped of its materials in four continuous steps and validated again.

The present study seeks to find the simplified structure of the human spine by employing fewer materials and assess the influence of each material part which are changed or omitted in the mechanical behavior of the human lumbar spine, along the process of testing by FE method. This method can be useful for making prosthesis and implanting easier, making another type of structure based on, especially for the future of building or joint due to its flexible and adapted natural form, and showing the way of developing, simplifying, and validating the other parts of human joints by FE method.

Materials and methods

In the present experimental analysis, the validated FE of two motion segments of the human lumbar spine (L3/L4) was made, and accordingly the simplification process was performed.

Making the validated FE of lumber spine (L3/L4)

The FE model was made based on the verified formula, properties, and techniques of validated models data [21, 33] in three main steps including the development of the geometric layout, material representation, and boundary and loading conditions [11, 35]. Then, the model was validated by comparing its data with the experimental validated data related to vivo, animal, artificial, and cadaveric spine models [21, 33]. According to the Dreischarf report, the combined simulation modeling data can be used to represent the predictive capability of the modeling [33].

Development of geometry

The two motion segments as a basic unit (having the complete character of the whole spine) was modelled step by step, through the combination of software (Fig. 1), with two vertebrae, intervertebral disc including annual matrix, annual fibres, nucleus, and endplates, ligaments, and facet joints [15].

First, the (2D) CT scan data as the basis for human lumbar vertebrae geometries, which is often used to create 3D models, with 3 mm slices from the vivo normal of a healthy person in an NRRD file format were imported into 3D Slicer software (3D Slicer 4.8.1) in order to be converted into a DICOM file format. Then, the model was imported into the MIMICS software (MIMICS Research 19.0) in order to generate 3D geometries of the vertebrae, separate the trabecular and cortical around 3 mm [36] by editing the CT scan data layer by layer, and make facet joints around 0.8 mm by filling the gaps between the two vertebrae [15], annuals matrix as the gap between two vertebrae [11] around 8 mm height including a nucleus in middle, nucleus around 40% of the intervertebral disc [17], and endplates around 0.8 mm [37] on the bottom surfaces of L3 and on the top surface of L4 vertebrae manually based on the CT scan of vertebrae in this software. Further, the 3D geometries with solo surface were copied to the 3-matic software (version 11.0) in order to make 10 tetrahedral volume, mesh (Table 1), and smooth the model. In the next procedure, the STL files formats of 3-matic software was imported into the Rhino software (Rhinoceros 5) to edit the geometry and add the annual fibres, which are defined by the lowest sections of the intervertebral disc in two layers of "x" shape [37, 38] ($\pm 10°$ to each other from the vertical axis). Further, the Rhino file (0.3 dm file format) was inserted into the space claim part of ANSYS (workbench 19.0) in order to add seven types of ligaments from node to node [39] of L3/L4 vertebrae. Finally, in the mechanical section of ANSYS, the ligaments nodes were
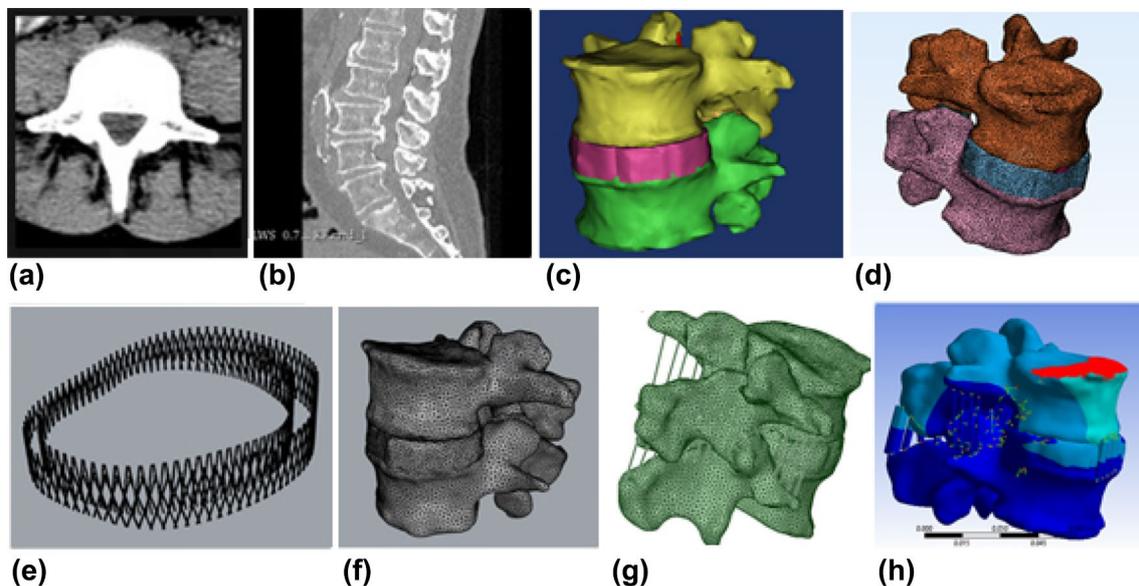
Fig. 1 **a** The CT scan data of Lumber, **b** getting the DICOM file in 3D slicer software, **c** getting the 3D form of L3/L4, Intervertebral disc, and facets shape in MIMICS software. **d** Making volume, smoothing, and meshing in 3-matic software. **e**, **f** Editing volume and making annuals fibers in Rhine software, **g** adding the ligaments in the space claim part of ANSYS software, **h** loading the bars in the mechanical part of ANSYS software

Table 1 The whole geometry properties of each part of two motion segments in ANSYS

Component	Properties		
	Node	Element	Area (L*W*H)
Cortical bone L3	158,105	91,872	0.098 * 0.096 * 0.053 m
Cortical bone L4	99,104	56,416	0.089 * 0.095 * 0.048 m
Trabecular Bone L3	42,601	24,875	0.048 * 0.038 * 0.027 m
Trabecular Bone L4	44,298	25,772	0.053 * 0.039 * 0.03 m
Cartilage endplate L3	15,517	7570	0.05 * 0.041 * 0.004 m
Cartilage endplate L4	11,347	5518	0.05 * 0.04 * 0.006 m
Nucleus	7588	4223	0.033 * 0.022 * 0.007 m
Annuals matrix	59,867	31,820	0.054 * 0.042 * 0.013–0.007 m
Annuals fiber 1	121,072	46,783	0.037 * 0.027 * 0.007 m
Annuals fiber 2	257,823	116,634	0.042 * 0.031 * 0.008 m
Facet joints 1	3073	1662	0.015 * 0.013 * 0.017 m
Facet joints 2	2879	1526	0.013 * 0.016 * 0.017 m
ALL	5*17	5*8	$5 * 12.56$ mm^2 (H: 0.014–0.018) m
PLL	5*17	5*8	$5 * 4.15$ mm^2 (H: 0.022–0.024) m
LF	4*17	5*8	$4 * 15.20$ mm^2 (H: 0.022–0.025) m
TL	8*17	8*8	$2 * 4 * 1.15$ mm^2 (H: 0.024–0.029) m
CL	20*17	20*8	$2 * 10 * 4.2$ mm^2 (H: 0.0007–0.0055) m
ISL	6*17	6*8	$6 * 7$ mm^2 (H: 0.0015–0.012) m
SSL	1*17	1*8	$1 * 3.14$ mm^2 (H: 0.018) m

attached to vertebrae as the fixed joints and apply the mesh to the ligaments (Fig. 1, Table 1).

Material properties

The materials were made in the material library section of the ANSYS program based on Modulus elasticity and Poisson's ratio for each geometry. Then, as shown in Table 2, the materials were applied to each geometry in the mechanical part of the ANSYS program [15, 16, 21, 36–38, 40–49].

Boundary and loading conditions

The loading conditions involved the combination of pure moment due to the directional movements and pure compression related to the local muscle forces and upper body weight by considering the movement directions of flexion, extension, lateral bending, and axial rotation of the two motion segments, which were derived from the validated resources for each direction (Fig. 2, Table 3) [33, 50]. In order to load these bars, the lowest part of the L4 vertebrae was fixed [39, 46] and the loads were applied on the top part of L3 vertebrae [11, 15, 21, 24, 36–38, 41, 48, 49].

Validation method

Validation was performed by measuring the internal and external response and their comparison with experimental vivo and vitro data. The Range of Motion (ROM), i.e. the

differences recorded between the angles of two vertebrae before and after loading the bars in degree represents the external response. The Intradiscal Pressure (IDP), as the amount of pressure in the midpoint of the nucleus in the intervertebral disc in MPa, indicates the internal response [33, 51]. In addition, the experimental vivo and vitro validated data for the human lumbar in the position of applying pure moments and compression have been addressed by different scholars which can be categorized into the following three groups as follow:

Group 1   Vitro data by Xu et al. for both ROM and IDP data [33]

Group 2   Vitro data by Ayturk and Puttlitz [28], Kiapour et al. [52], Little et al. [27], Liu et al. [53], Park et al. [32], Schmidt et al. [29], Shirazi-Adl [54], and Zander et al. [55] for both ROM and IDP data [50]

Group 3   Vivo data by Pearcy et al. [56], Pearcy and Tibrewal (1984) [57], and Pearcy [58] for ROM data and the vivo data by Wilke et al. for IDP data [33, 50, 59].

Diagrams 1 and 2 display the comparison of the FE model related to two motion segments of the human lumbar spine with previous experimental vivo and vitro data. The experimental vivo and vitro data of ROM and IDP in these diagrams indicate an appropriate range of standard

Table 2 The material properties

Component	Element			Material properties			
	Type	Form	Area of contact (mm2)	E (MPa)	V	Formulation	
Cortical bone	10 node tetrahedral (solid)	Solid	CT scan data	12,000	0.3	Linear	Isotropic
Trabecular Bone	10 node tetrahedral (solid)	Solid	CT scan data	140	0.2	Linear	Isotropic
Cartilage endplate	10 node tetrahedral Hyper elastic	Mooney-Rivlin[a]	Based on CT scan data	10.4	0.4	Linear	Isotropic
Nucleus	10 node tetrahedral Hyper elastic	Mooney-Rivlin[a]	40% of Annuals matrix	1	0.49	Linear	Isotropic
Annuals matrix (reinforced by collagen annuals fibers)	10 node tetrahedral Hyper elastic	Mooney-Rivlin[a]	Based on CT scan data	4.2	0.45	Linear	Isotropic
Annuals fiber 1	10 node tetrahedral Hyper elastic Truss	Mooney-Rivlin[a]	–	350	0.3	Linear	Isotropic
Annuals fiber 2	10 node tetrahedral Hyper elastic Truss	Mooney-Rivlin[a]	–	455	0.3	Linear	Isotropic
Facet Joints	10 node tetrahedral Hyperelastic	Mooney-Rivlin[a]	Based on CT scan data	12	0.4	Linear	Isotropic
ALL	Beam–Tension only	Neo-Hookean[b]	5 * 12.56	10	0.3	Nonlinear	isotropic
PLL	Beam–Tension only	Neo-Hookean[b]	5 * 4.15	20	0.3	Nonlinear	Isotropic
LF	Beam–Tension only	Neo-Hookean[b]	4 * 15.20	10	0.3	Nonlinear	Isotropic
TL	Beam–Tension only	Neo-Hookean[b]	2 * 4 * 1.15	20	0.3	Nonlinear	Isotropic
CL	Beam–Tension only	Neo-Hookean[b]	2 * 10 * 4.2	20	0.3	Nonlinear	Isotropic
ISL	Beam–Tension only	Neo-Hookean[b]	1 * 7	10	0.3	Nonlinear	Isotropic
SSL	Beam–Tension only	Neo-Hookean[b]	6 * 3.14	10	0.3	Nonlinear	Isotropic

ALL anterior longitudinal ligament, *PLL* posterior longitudinal ligament, *FL* flaval ligament, *CL* facet capsular ligament, *ITL* intertransverse ligament, *ISL* interspinous ligament, and *SSL* supraspinous ligament

[a]Because of having the role of fluid

[b]Due to being not compressed material

deviation for validating the data. Thus, the validity of the data is confirmed for each type of study and analysis [33].

Simplifying the material of two motion segments

To make the simplified structure for future modeling, the two motion segments should be simplified in four continuous steps in order to evaluate the effect of each material in the behavior of the two motion segments. In each step, the changes added to the previous steps are not considered instead. The ROM and IDP data were derived for analysis and validation. Further, the stress and strain curves were derived for analysis.

Step 1   Simplify two motion segments by omitting the annual fibers of the annual matrix which work just in extension.

Step 2   Simplify two motion segments without annual fibers by representing the material of annual matrix to the nucleus part of the intervertebral disc to make the integrated intervertebral disc.

Step 3   Simplify two motion segments without annual fibers by representing the same material of annual matrix material to nucleus and endplates to make a better integrated intervertebral disc.

Step 4   Simplify two motion segments without annual fibers and the same material for annual, nucleus, and endplate by omitting the trabecular parts of vertebrae to make the light structure during the last step of simplification in the material part of the structure in two motion segments.

Results

All of the results related to the validated model and simplified models were based on the model under pure compression and moments according to its directions including flexion, extension, lateral bending, and axial rotation. The equivalent von-mises stress was calculated due to the hydraulic behavior of the intervertebral disc and facets joints[33]. Diagrams 1 and 2 display the amount of the IDP and ROM data for the validated FE model of two motion segments of the human lumbar spine in all four directions. Diagrams 3, 4, 5, and 6 illustrate the comparison of the analyzed data related to IDP, ROM, stress curve, and strain curve for all four positions of flexion, extension, lateral bending, and axial rotation in the ANSYS software for four continuous simplified steps.
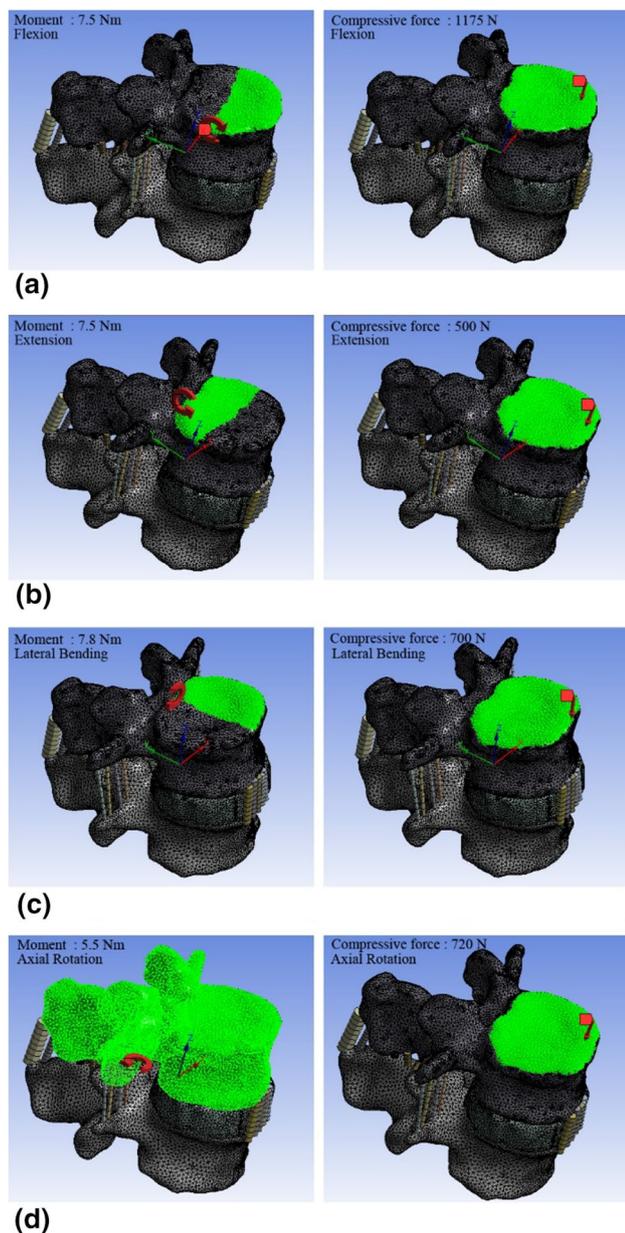
Fig. 2 **a** The combined loads of flexion, **b** the combined loads of extension, **c** the combined loads of lateral bending, **d** the combined loads of axial rotation

Table 3 The amount of Loads

Body position	Compressive force (N)	Moment (Nm)
Flexion	1175	7.5
Extension	500	7.5
Lateral bending	700	7.8
Axial Rotation	720	5.5

Step 1: the two motion segments without annual fibers

By omitting the annuals fibers which just function in extension, the IDP of 1.057, 0.187, 0.529, and 0.528 MPa, and ROM of 1.20, 0.118, 0.78, and 0.6° were obtained for flexion, extension, lateral bending, and axial rotation, respectively. The stress and strain curves indicated that the maximum stress of 77.3 MPa occurs in a cortical part of L3 in the lateral bending direction while the maximum strain of 1.32 m/m happens in the annual part of the flexion.

Step 2: representing the material of annual to the nucleus

By changing the material of the nucleus by representing the material of annual to make the simple intervertebral disc, the IDP of 1.55, 0.187, 077, and 0.76 MPa, and ROM of 1.15°, 0.12°, 0.74°, and 0.54° were obtained for flexion, extension, lateral bending, and axial rotation, respectively. The stress and strain curves showed that the maximum stress of 73.9 MPa happens in a cortical part of L3 in the lateral bending direction while the maximum strain of 1.23 m/m occurs in the annual part of the flexion.

Step 3: representing the material of annual to the endplates

The IDP of 1.54, 0.267, 0.772, and 0.768 MPa, and ROM of 1.27°, 0.105°, 0.83°, and 0.6° were obtained for flexion, extension, lateral bending, and axial rotation, respectively, by changing the material of the endplates similar to the previous step by representing the material of annual to make the intervertebral disc with one material. Based on the stress and strain curves, the maximum stress of 81.8 MPa happens in a cortical part of L3 in the lateral bending direction and the maximum strain of 1.78 m/m occurs in the annual part of the flexion.

Step 4: omitting the trabecular part of vertebrae

The IDP of 1.495, 0.263, 0.747. 0.741 MPa, and ROM of 1.23°, 0.105°, 0.77°, 0.52° were obatined for flexion, extension, lateral bending, and axial rotation, respectively, by omitting the trabecular part of vertebrae to make the light structure with one material. The stress and strain curves indicated that the maximum stress of 83 MPa happens in the cortical part of L3 in the lateral bending direction and the maximum strain of 1.82 m/m occurs in the annual part of the flexion.

Diagram 1 Intradiscal pressure (IDP) for two motion segments of this study in compare of the other studies in **a** flexion, **b** extension, **c** lateral bending, and **d** axial rotation
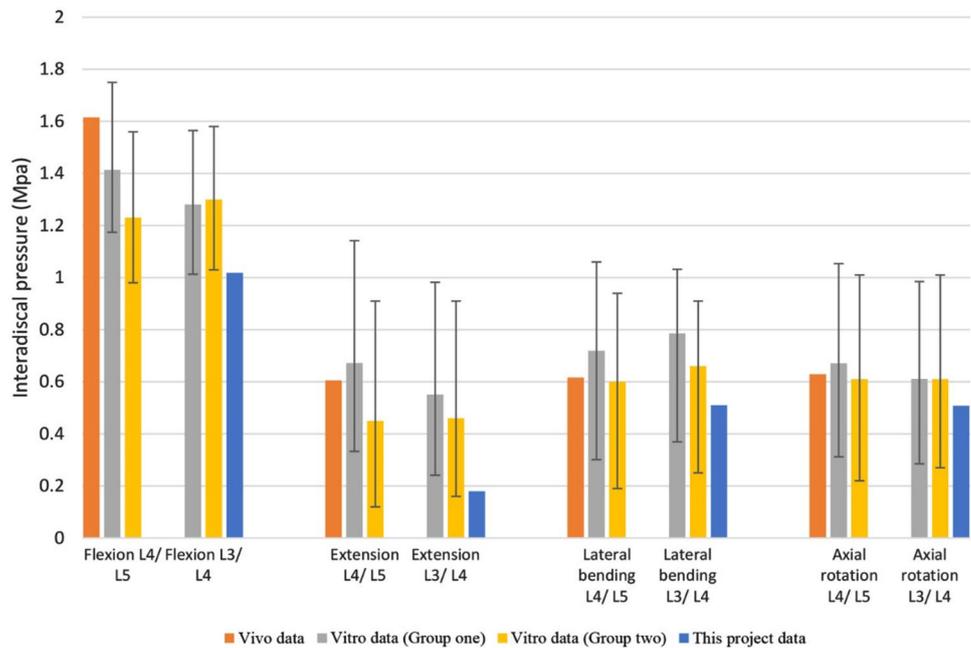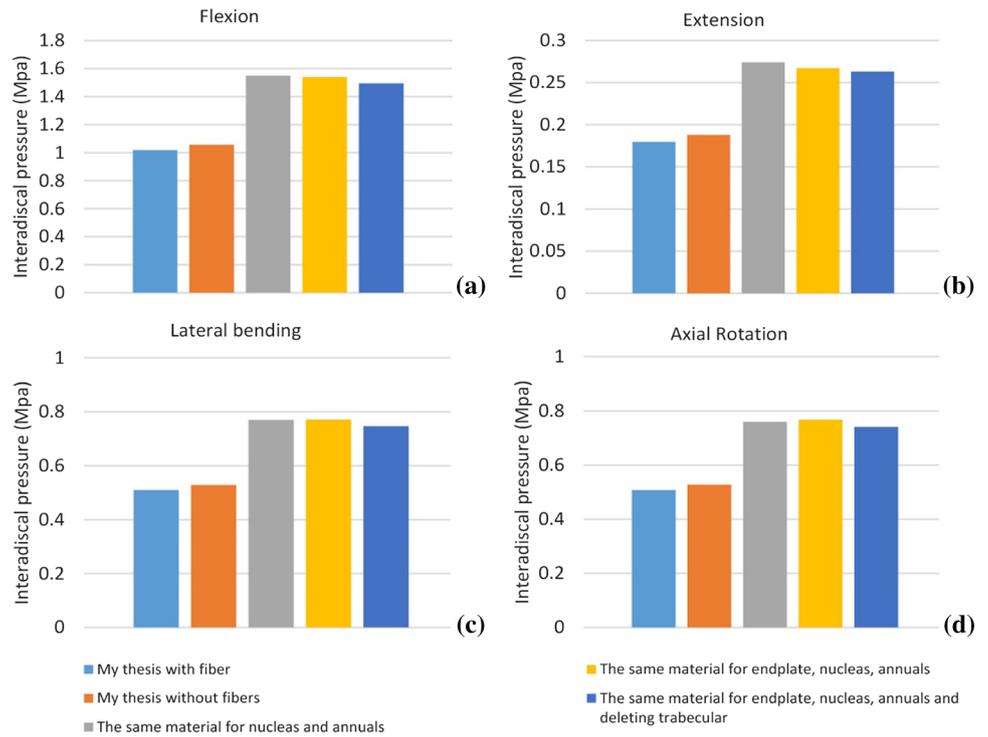

Diagram 2 Range of motion (ROM) for two motion segments of this study in compare of the other studies in **a** flexion, **b** extension, **c** lateral bending, and **d** axial rotation
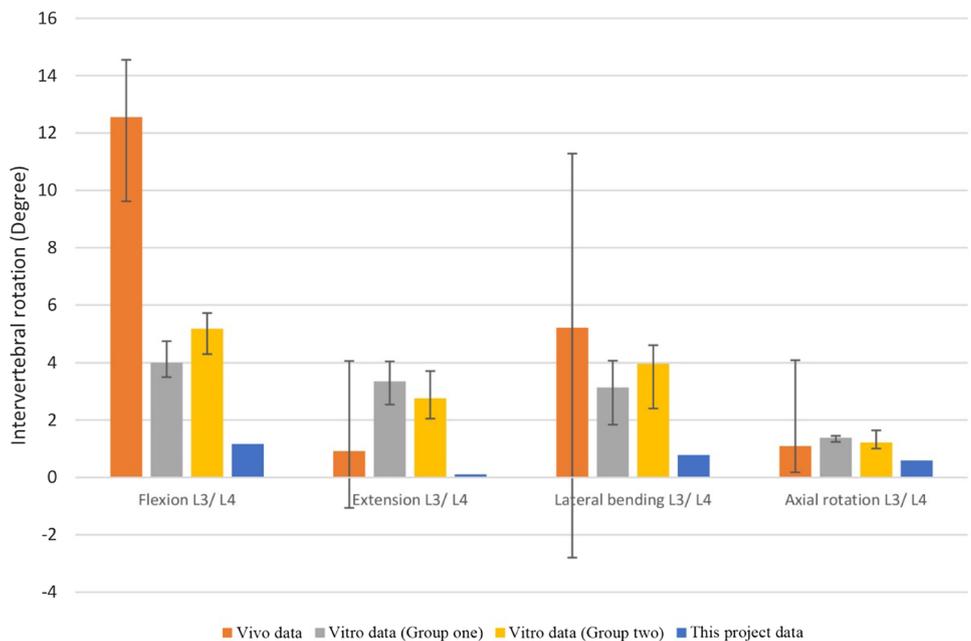

Discussion

As shown in Diagrams 1 and 2, the FE model of the L3/L4 before simplification was validated under both pure compression and moment in four directions of flexion, extension, lateral bending, and axial rotation by checking its internal (IDP) and external response (ROM) with the experimental vivo and vitro data [33, 50]. According to the IDP diagram in Diagram 1, the flexion and extension IDP data seem to be closer to the minimum data of group 1 and 2 vitro data

(1 ± 0.05 MPa and 0.2 ± 0.05 MPa for flexion and extension, respectively) [27–29, 32, 33, 50, 52–55], while they have 0.6 and 0.4 MPa differences with the flexion and extension IDP vivo data for human lumbar spine L4/L5 for the lack of vivo IDP data for L3/l4, respectively, obtained by Wilke et al.[59] (Diagram 1a, b). Further, the lateral bending and axial rotation IDP data are closer to the median of both the vitro (Group 1 and 2) [27–29, 32, 33, 50, 52–55] and vivo IDP experimental data (0.6 MPa, 0.6 MPa for lateral bending and axial rotation, respectively), as reported Wilke et al.

Diagram 3 Intradiscal pressure (IDP) for two motion segments in four steps of material simplifications in **a** flexion, **b** extension, **c** lateral bending, and **d** axial rotation


Diagram 4 Range of motion (ROM) for two motion segments in four steps of material simplifications in **a** flexion, **b** extension, **c** lateral bending, and **d** axial rotation
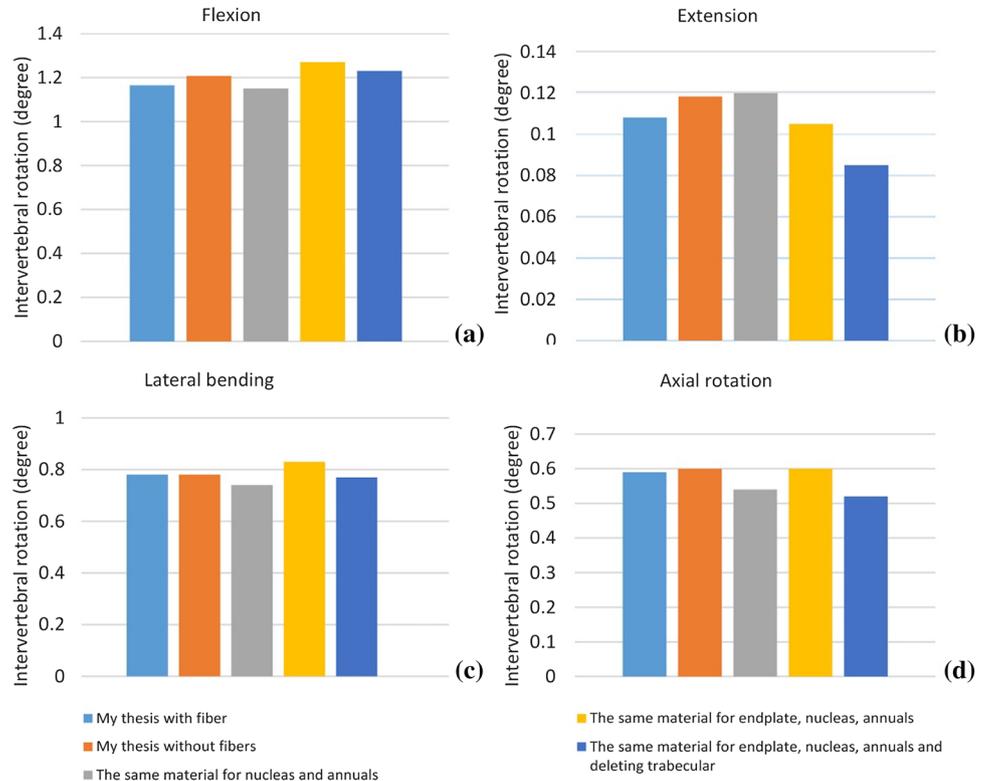
[59] (Diagram 1c, d). In summary, all the IDP data are validated since they all appear in the standard deviation range of experimental vitro data. As shown in the ROM in Diagram 2 for FE of human lumbar spine, all ROM data are lower than

the vitro ROM data of groups 1 and 2 in all four directions of flexion, extension, lateral bending, and axial rotation in the degrees of −3, −2, −3, and −0.5, respectively [27–29, 32, 33, 50, 52–55], while all these ROM data except flexion

Diagram 5 Stress curves for two motion segments in four steps of material simplifications in **a** flexion, **b** extension, **c** lateral bending, and **d** axial rotation
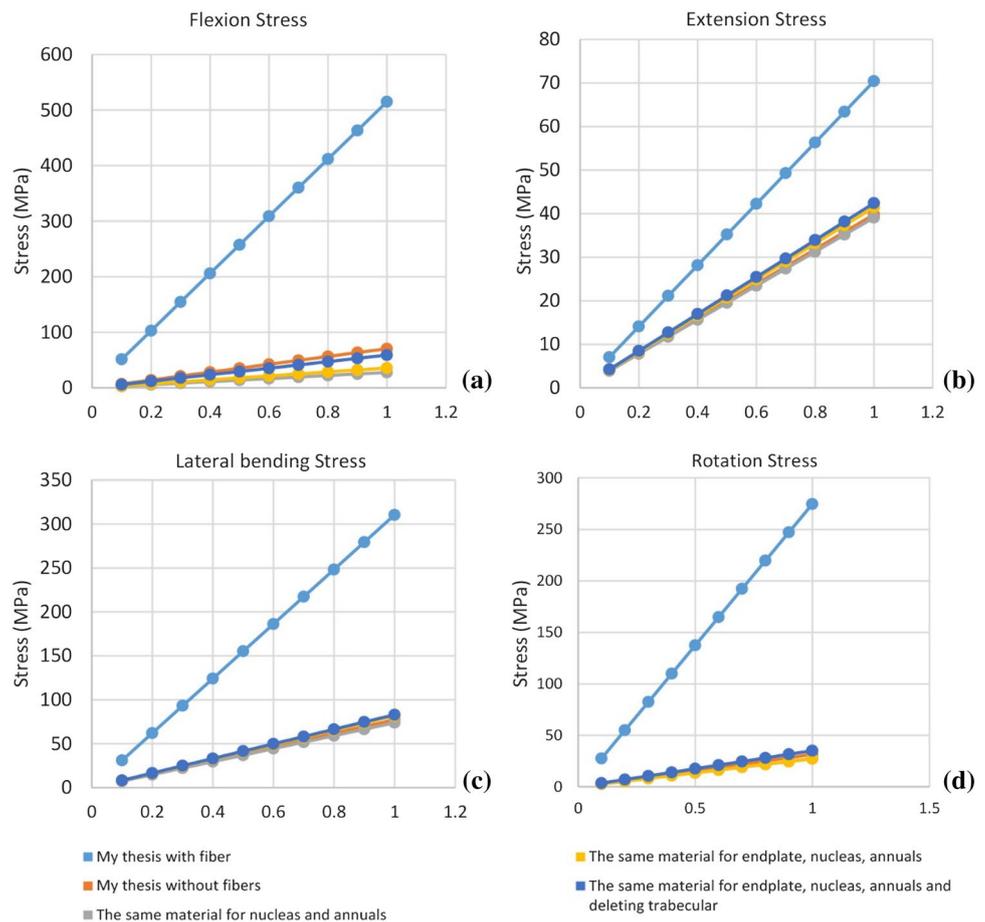
(−12°) are in the range of vivo data, as reported by Pearcy et al. [57], Pearcy and Tibrewal [57], and Pearcy [58] (Diagram 2b, c, and d). Like ROM experimental vitro data for flexion (−8°) [27–29, 32, 33, 50, 52–55], the present ROM data for flexion has more difference with the experimental vivo ROM data by some researchers (Pearcy et al. [56], Pearcy and Tibrewal [57], and Pearcy [58]in flexion data (Diagram 2a). Thus, the most ROM data were in the standard deviation range of vivo validating data except for ROM data in the flexion direction in which some differences were observed between its vivo and vitro data in the experimental validation data (the range of the validatation vitro data was out of the range of vivo data in flexion ROM data). The difference in the results was expected given some characteristics related to source data such as sex, age, level of degeneration, and specimens [50], and different types of CT scan (CT scan machine and distance between CT scan slices), as well those in the experimental setup. Finally, the model was validated since most of the data were found in the standard deviation range of the experimental vivo or vitro data. The maximum stress and strain happened in inner annual fibers while the minimum occurred in outer annual fibers in all four directions of flexion, extension, lateral bending, and axial rotation.

In addition, the simplifications of the materials were observed on the validated FE model of human lumbar spine L3/L4 in four continuous steps (Diagrams 3, 4, 5, and 6). As shown in the IDP diagrams, the result in each step is similar (less than 5% compared to the previous step) except between steps one and two (changing the material of nucleus), which have 0.4, 0.1, 0.25, and 0.24 MPa differences in the directions of flexion, extension, lateral bending, and axial rotation, respectively. Based on these differences, an increase of approximately 50% is observed, since the changes in the nucleus material and IDP indicates the amount of pressure in the nucleus part (Diagram 3). Despite the degree of difference with FE model of this study, all these data of IDP are in the standard deviation range of the experimental vivo data by Wilke et al. [59] and vitro data in group 1 and 2 [27–29, 32, 33, 50, 52–55], as shown in Diagram 1. Based on the ROM diagrams, all of the data in the four steps of simplifications are closer to each other (±0.05° near the 5%) (Diagram 4). Based the similarities in ROM and IDP data in each direction except the IDP between the steps one and two, which are in the range of experimental vivo and vitro data, these data were validated indicating a promising approach towards material simplifications for further structure based on the human lumbar spine L3/L4.

Diagram 6 Strain curves for two motion segments in four steps of material simplifications in **a** flexion, **b** extension, **c** lateral bending, and **d** axial rotation
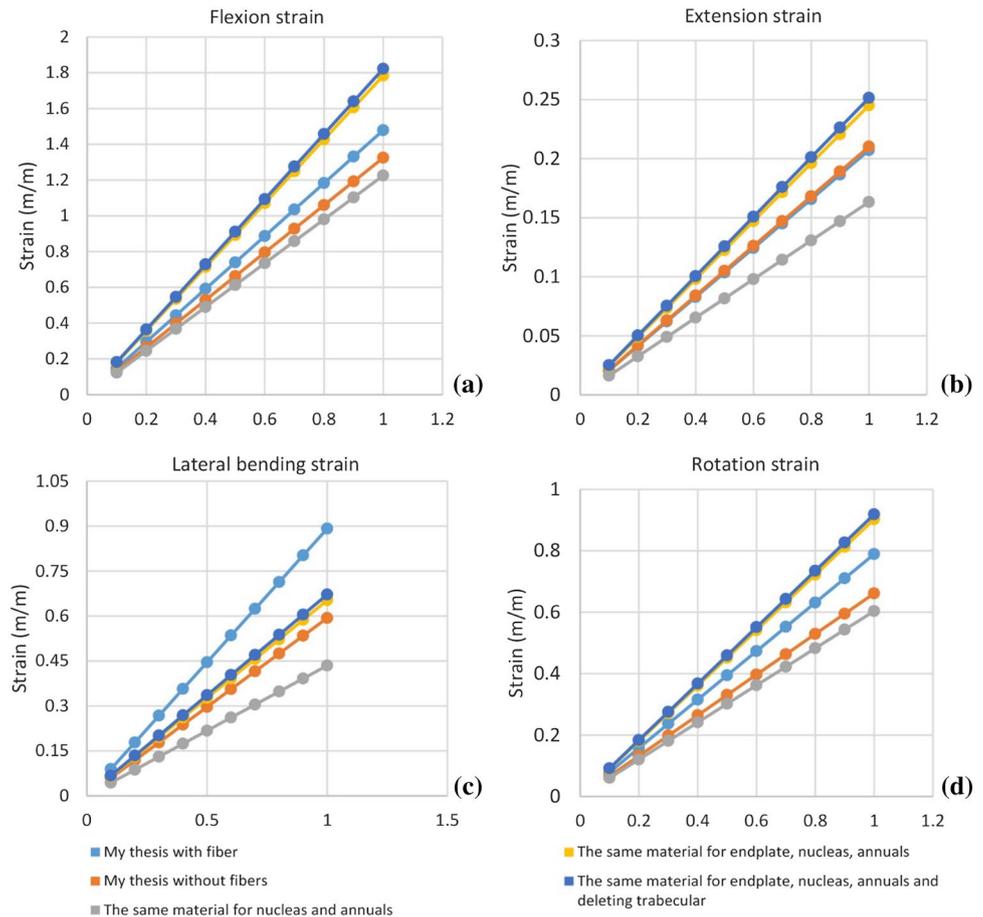
As illustrated in Diagram 5, based on the stress curve, in all of the continuous steps except the step one, the same stress data ($\pm 5\%$) are observed while a considerable decrease occurs in the steps 1 to 2 by omitting the annual fibers i.e. a reduction of 500, 30, 250, and 250 MPa around -90%, -50%, -75%, and -90% for flexion, extension, bending and rotation, respectively. In addition, the maximum stress changes from the annual fibers to the cortical part of L3, which can be related to omitting the annual fibers. Further, the reduction in stress results in simulating method for further structure due to less stress in the further models. As illustrated in Diagram 6, the strain curve indicated that the results have a variance of $\pm 0.4, \pm 0.1, \pm 0.1$, and ± 0.3 m/m ($\pm 40\%, \pm 25\%, \pm 35\%$, and $\pm 25\%$) with the normal FE model data for flexion, extension, bending and rotation, respectively. Furthermore, the maximum strain change was observed in the maximum strain from the annual fiber to the annual part in all of the four continuous steps except the extension and lateral bending directions of solo in the step 1, the maximum strain of which is in the nucleus part.

By simplifying the material of the human lumbar spine and validating its data, it is possible to develop the structure with the anatomical and mechanical role of human lumbar spine but only with four main parts of cortical bone instead of the whole vertebrae, as well as the annual matrix instead of a the whole intervertebral disc, ligaments, and facet joints. Therefore, the way of changing one part of two motion segments with prosthesis or making the structure based on this structure for both aspects of implanting or building joints reduces the time by material considerations of FE modeling.

Conclusion

The basic model for the implants, prosthesis, structures, and modeling in the human lumbar spine has been developed from the validated FE model of the standard human lumbar spine. The FE of the human lumbar spine was made based on CT scan data as the foundation for the vertebrae geometry, verified geometry data for making the other parts of two motion segments manually, and verified material data. In addition, the FE model was designed under the combination bars of pure compression and moments in four directions of flexion, extension, lateral bending, and axial rotation. Then, the human lumbar spine was simplified in material parts in four steps of omitting the annual fiber (annual fibers just

work in extension), representing the annual matrix material to nucleus, demonstrating the annual matrix material to endplates, and omitting the trabecular part of vertebrae in order to make the light structure in a series of continuous steps. Accordingly, the data obtained from the analysis were checked for ROM and IDP based on the validated normal model data in order to analyze their internal and external response against the loads in different directions and obtain their stress and strain curves. Based on the results, the ROM and IDP data are generally consistent with the normal FE model as basic FE model in each direction except the IDP between the steps 1 and 2, which are in the range of experimental validated vivo and vitro data. Further, the modeling method introduced in this study was valid for describing an accurate building design of simple structure based on the anatomic and biomechanics of the human lumbar spine. Furthermore, the validated method can be used in future lumbar spine models for making a prosthesis, implant, or treating the lumbar diseases, and using in architecture driven based on nature approaches and in planning industrial spaces. Additionally, it can inspire structural configurations which are aesthetically satisfactory, while offering modular solutions for lightweight, dynamic, and stable structure. The human lumbar spine is considered as an example of many structures within the human body which can potentially influence future modeling and construction technique toward better-integrated solutions.

Compliance with ethical standards

Conflict of interest All authors declared that they have no conflict of interest.

Ethical approval This article does not involve any studies with human participants or animals performed by any of the authors.

Informed consent Informed consent was obtained from all individual participants included in the study.

References

1. Lebedev YS, Stroiizdat M (1990) Bionic architecture. Stroiizdat, Moscow p, p 269
2. Salsabili N, Mahmoudi MM, Salsabili N, Nasr Azadani A (2016) Designing structural systems based on the hip joint. In 4th international conference on civil and architectural engineering Ur pp 1–17
3. Salsabili N, Prieto Barrio MI, Santiago López J (2018) Human Joints as a beneficial source of building structure. CITE 2018
4. Versos CAM, Coelho DA (2011) Biologically inspired design: methods and validation. Ind Des Front 101:120. https://doi.org/10.5772/20326
5. Types of Joints. https://www.teachpe.com/anatomy/joints.php. Accessed 1 Aug 2017
6. Zakharchuk A (2012) Bionics in architecture. Chall Mod Technol 3:50–53
7. Taghizadeh K, Bastanfard M (2012) The anatomy of a human body, a model to design smart high building. Sci Technol 2:8–14
8. Salsabili N (2014) Designing constructive systems based on the spine structure. Adv Environ Biol 8:1324–1337
9. Al-Obaidi KM, Ismail MA, Hussein H, Rahman AMA (2017) Biomimetic building skins: an adaptive approach. Renew Sustain Energy Rev 79:1472–1491
10. Ajay Harish Finite Element Method – What Is It? FEM and FEA Explained. https://www.simscale.com/blog/2016/10/what-is-finite-element-method/. Accessed 1 May 2018
11. Zafarparandeh I, Erbulut DU, Lazoglu I, Ozer AF (2014) Development of a finite element model of the human cervical spine. Turk Neurosurg 24:312–318
12. Finite Element Analysis (FEA). https://www.plm.automation.siemens.com/global/en/our-story/glossary/finite-element-analysis-fea/13173. Accessed 1 May 2018
13. Introduction to finite element analysis. https://www.open.edu/openlearn/science-maths-technology/introduction-finite-element-analysis/content-section-1.5. Accessed 1 May 2018
14. FEA software. https://www.autodesk.com/solutions/finite-element-analysis#. Accessed 1 Aug 2017
15. Tyndyk MA, Barron V, McHugh PE, Mahoney D (2007) Generation of a finite element model of the thoracolumbar spine. Acta Bioeng Biomech 9:35
16. Toosizadeh N, Haghpanahi M (2011) Generating a finite element model of the cervical spine: estimating muscle forces and internal loads. Sci Iran 18:1237–1245
17. Aroeira RMC, Pertence AE, Kemmoku DT, Greco M (2017) Three-dimensional geometric model of the middle segment of the thoracic spine based on graphical images for finite element analysis. Res Biomed Eng 33:97–104
18. Salsabili N, Prieto Barrio MI, Santiago López J (2019) Model development by Finite Element method. CITE 2019
19. Fagan MJ, Julian S, Siddall DJ, Mohsen AM (2002) Patient-specific spine models. Part 1: finite element analysis of the lumbar intervertebral disc—a material sensitivity study. Proc Inst Mech Eng Part H 216:299–314
20. Finite Element Analysis. https://www.simscale.com/docs/content/simwiki/fea/whatisfea.html. Accessed 1 Aug 2017
21. Ha SK (2006) Finite element modeling of multi-level cervical spinal segments (C3–C6) and biomechanical analysis of an elastomer-type prosthetic disc. Med Eng Phys 28:534–541
22. Zhang QH, Teo EC (2008) Finite element application in implant research for treatment of lumbar degenerative disc disease. Med Eng Phys 30:1246–1256
23. The Finite Element Method (FEM). https://www.comsol.es/multiphysics/finite-element-method. Accessed 1 May 2018
24. Du H, Liao S, Jiang Z, Huang H, Ning X, Jiang N, Pei J, Huang Q, Wei H (2016) Biomechanical analysis of press-extension technique on degenerative lumbar with disc herniation and staggered facet joint. Saudi Pharm J 24:305–311
25. Anatomy and Function. https://www.umm.edu/programs/spine/health/guides/anatomy-and-function. Accessed 1 Aug 2017
26. Shirazi-Adl A (1994) Analysis of role of bone compliance on mechanics of a lumbar motion segment. J Biomech Eng 116:408–412
27. Little JP, De Visser H, Pearcy MJ, Adam CJ (2008) Are coupled rotations in the lumbar spine largely due to the osseo-ligamentous

anatomy? A modeling study. Comput Methods Biomech Biomed Engin 11:95–103

28. Ayturk UM, Puttlitz CM (2011) Parametric convergence sensitivity and validation of a finite element model of the human lumbar spine. Comput Methods Biomech Biomed Engin 14:695–705

29. Schmidt H, Galbusera F, Rohlmann A, Zander T, Wilke H-J (2012) Effect of multilevel lumbar disc arthroplasty on spine kinematics and facet joint loads in flexion and extension: a finite element analysis. Eur Spine J 21:663–674

30. Kiapour A, Anderson DG, Spenciner DB, Ferrara L, Goel VK (2012) Kinematic effects of a pedicle-lengthening osteotomy for the treatment of lumbar spinal stenosis. J Neurosurg Spine 17:314–320

31. Lin H-M, Pan Y-N, Liu C-L, Huang L-Y, Huang C-H, Chen C-S (2013) Biomechanical comparison of the K-ROD and Dynesys dynamic spinal fixator systems—a finite element analysis. Biomed Mater Eng 23:495–505

32. Park WM, Kim K, Kim YH (2013) Effects of degenerated intervertebral discs on intersegmental rotations, intradiscal pressures, and facet joint forces of the whole lumbar spine. Comput Biol Med 43:1234–1240

33. Xu M, Yang J, Lieberman IH, Haddas R (2017) Lumbar spine finite element model for healthy subjects: development and validation. Comput Methods Biomech Biomed Engin 20:1–15

34. Little JP, Adam CJ (2015) Geometric sensitivity of patient-specific finite element models of the spine to variability in user-selected anatomical landmarks. Comput Methods Biomech Biomed Engin 18:676–688

35. Prof. Olivier de Weck DIYK Finite element method. https://en.wikipedia.org/wiki/Finite_element_method. Accessed 1 Aug 2017

36. Kuo C-S, Hu H-T, Lin R-M, Huang K-Y, Lin P-C, Zhong Z-C, Hseih M-L (2010) Biomechanical analysis of the lumbar spine on facet joint force and intradiscal pressure-a finite element study. BMC Musculoskelet Disord 11:151

37. Maurel N, Lavaste F, Skalli W (1997) A three-dimensional parameterized finite element model of the lower cervical spine, study of the influence of the posterior articular facets. J Biomech 30:921–931

38. Kumaresan S, Yoganandan N, Pintar FA, Maiman DJ (1999) Finite element modeling of the cervical spine: role of intervertebral disc under axial and eccentric loads. Med Eng Phys 21:689–700

39. Vikram Subramani JJ (2016) The Development and Analysis of a Finite Element Model of the C45 Cervical Spine Segment Group Members: Dep Mech Nucl Eng Univ Park PA

40. Sahani R (2015) Finite element analysis of human lumbar vertebrae in pedicle screw fixation

41. Schmidt H, Heuer F, Simon U, Kettler A, Rohlmann A, Claes L, Wilke H-J (2006) Application of a new calibration method for a three-dimensional finite element model of a human lumbar annulus fibrosus. Clin Biomech 21:337–344

42. Li Y, Fogel GR, Liao Z, Tyagi R, Zhang G, Liu W (2017) Biomechanical analysis of two-level cervical disc replacement with a stand-alone U-shaped disc implant. Spine (Phila Pa 1976) 42:1173–1181

43. Salvatore G, Berton A, Giambini H, Ciuffreda M, Florio P, Longo UG, Denaro V, Thoreson A, An K-N (2018) Biomechanical effects of metastasis in the osteoporotic lumbar spine: a Finite Element Analysis. BMC Musculoskelet Disord 19:38

44. Lee KK, Teo E-C, Fuss FK, Vanneuville V, Qiu T-X, Ng H-W, Yang K, Sabitzer RJ (2004) Finite-element analysis for lumbar interbody fusion under axial loading. IEEE Trans Biomed Eng 51:393–400

45. Ibarz E, Herrera A, Más Y, Rodríguez-Vela J, Cegoñino J, Puértolas S, Gracia L (2012) Development and kinematic verification of a finite element model for the lumbar spine: application to disc degeneration. Biomed Res Int 2013:705185

46. Wu JSS, Chen JH (1996) Clarification of the mechanical behaviour of spinal motion segments through a three-dimensional poroelastic mixed finite element model. Med Eng Phys 18:215–224

47. Zhang QH, Teo EC, Ng HW, Lee VS (2006) Finite element analysis of moment-rotation relationships for human cervical spine. J Biomech 39:189–193

48. Noailly J, Lacroix D, Planell JA (2003) The mechanical significance of the lumbar spine components—a finite element stress analysis. In: Proceedings of the summer bioengineering conference

49. Ben-Hatira F, Saidane K, Mrabet A (2012) A finite element modeling of the human lumbar unit including the spinal cord. J Biomed Sci Eng 5:146

50. Dreischarf M, Zander T, Shirazi-Adl A, Puttlitz CM, Adam CJ, Chen CS, Goel VK, Kiapour A, Kim YH, Labus KM (2014) Comparison of eight published static finite element models of the intact lumbar spine: predictive power of models improves when combined together. J Biomech 47:1757–1766

51. Campbell JQ, Coombs DJ, Rao M, Rullkoetter PJ, Petrella AJ (2016) Automated finite element meshing of the lumbar spine: verification and validation with 18 specimen-specific models. J Biomech 49:2669–2676

52. Kiapour A, Ambati D, Hoy RW, Goel VK (2012) Effect of graded facetectomy on biomechanics of Dynesys dynamic stabilization system. Spine (Phila Pa 1976) 37:581–589

53. Liu C-L, Zhong Z-C, Hsu H-W, Shih S-L, Wang S-T, Hung C, Chen C-S (2011) Effect of the cord pretension of the Dynesys dynamic stabilisation system on the biomechanics of the lumbar spine: a finite element analysis. Eur Spine J 20:1850–1858

54. Shirazi-Adl A (1994) Biomechanics of the lumbar spine in sagittal/lateral moments. Spine (Phila Pa 1976) 19:2407–2414

55. Zander T, Rohlmann A, Bergmann G (2009) Influence of different artificial disc kinematics on spine biomechanics. Clin Biomech 24:135–142

56. Pearcy M, Portek IAN, Shepherd J (1984) Three-dimensional x-ray analysis of normal movement in the lumbar spine. Spine (Phila Pa 1976) 9:294–297

57. Pearcy MJ, Tibrewal SB (1984) Axial rotation and lateral bending in the normal lumbar spine measured by three-dimensional radiography. Spine (Phila Pa 1976) 9:582–587

58. Pearcy MJ (1985) Stereo radiography of lumbar spine motion. Acta Orthop Scand 56:1–45

59. Wilke H-J, Neef P, Hinz B, Seidel H, Claes L (2001) Intradiscal pressure together with anthropometric data–a data set for the validation of models. Clin Biomech 16:S111–S126